ACS Catalysis

pubs.acs.org/acscatalysis
Research Article

The Promoting Effect of Mg on Propane Dehydrogenation over Co/Silicalite-1 Catalysts

Xiangnong Ding, Qiyang Zhang,* Dmitry E. Doronkin, Stephan Bartling, Henrik Lund, Dongxu Wang, Elizaveta Fedorova, Christoph Kubis, and Evgenii V. Kondratenko*

Cite This: ACS Catal. 2026, 16, 8543−8554

ABSTRACT: Non-oxidative dehydrogenation of propane (PDH) is a well-established large-scale route for on-purpose propene production. Cobalt-based catalysts have attracted increasing attention due to their attractive performance as environmentally friendly and cost-efficient alternatives to commercially used catalysts containing chromium or platinum. However, their further development to reach an industrially attractive level is hindered by insufficient knowledge of the structure-activity-selectivity relationships for tailored catalyst design and preparation. In this work, magnesium (Mg) is introduced as a promoter to regulate the local structure of CoO_x species on the surface of silicalite-1. Owing to the formation of Co−O−Mg bond(s) in the presence of the promoter, the formed CoO_x species become isolated, less reducible, and less acidic. These changes are key to catalyst activity and propene selectivity. The promoter effectively decreases the amount of strong acidic sites, thereby facilitating propene desorption and accordingly suppressing undesired cracking and deep dehydrogenation reactions involving adsorbed propene. The optimized catalyst outperforms an analogue of commercial K-CrO_x/Al_2O_3 and demonstrates durability in a series of five PDH/regeneration cycles under industrially relevant conditions. The space-time yield of propene formation reached 1.2 $kg_{C3H6}{\cdot}kg_{cat}^{-1}{\cdot}h^{-1}$ at 550 °C and 68% of the equilibrium propane conversion, being higher in comparison to that of most previously reported cobalt-based catalysts under comparable conditions. In view of this result, the structural and mechanistic knowledge obtained on the promoter effect can be used to prepare highly efficient PDH catalysts with supported metal-oxide species, including those beyond CoO_x.

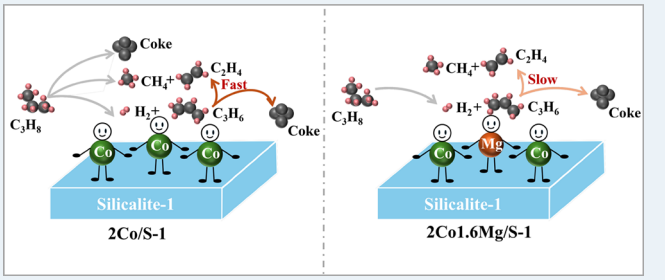

KEYWORDS: *propane, dehydrogenation, cobalt, Mg modification, reaction pathways*

INTRODUCTION

Propene is one of the most important building blocks in the chemical industry, which can be converted into polypropylene, acrylic acid, acetone, and other industrially important products.[1−3] Nowadays, petroleum-based processes, such as fluid catalytic cracking and steam cracking, provide a major part of propene.[1] However, due to the low selectivity to propene in these processes and the limited oil reserves, the traditional propene production can no longer meet the global demand.[4,5] To bridge the gap between the demand and the supply of propene, alternative technologies such as non-oxidative propane dehydrogenation (PDH),[6−11] methanol-to-olefins (MTO),[12,13] have been developed. The former approach has become increasingly attractive due to the exploitation of shale gas, which makes the feedstock (propane) cheaper and plentiful.[1] However, the major PDH technologies like Oleflex and Catofin using Pt- and Cr-based catalysts suffer from the high cost of Pt and the toxicity of Cr (VI) compounds, respectively.[1,14,15] These drawbacks have driven the development of low-cost and eco-friendly catalysts with high activity, propene selectivity, durability and on-stream stability.

Co-based catalysts have been considered as one of the most promising alternatives.[16−21] Highly dispersed Co^{2+} species on the surface of supports, including Al_2O_3,[22,23] SiO_2,[24] ZrO_2,[8] and zeolite[20,25] are widely recognized to be responsible for the efficient dehydrogenation of propane. For example, Li et al. reported that highly dispersed metallic Co particles on the surface of silicalite-1 (S-1) achieved a space-time-yield of propene formation (STY(C_3H_6)) of 1.5 $kg_{C3H6}{\cdot}kg_{cat}^{-1}{\cdot}h^{-1}$ with a propene selectivity of 95%.[26] However, this catalyst failed to restore its initial activity after regeneration in air at 550 °C. This group later demonstrated that catalysts with isolated $Co^{2+}O_x$ supported on the surface of ZrO_2 are durable at 550 °C but have a lower STY(C_3H_6) of 0.71 $kg_{C3H6}{\cdot}kg_{cat}^{-1}{\cdot}h^{-1}$ and a lower

Received: February 8, 2026
Revised: March 28, 2026
Accepted: April 9, 2026
Published: April 16, 2026

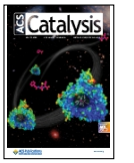

https://doi.org/10.1021/acscatal.6c01078
ACS Catal. 2026, 16, 8543−8554

propene selectivity of 81%.[8] Wang et al. also constructed isolated $Co^{2+}O_x$ supported on the SiO_2 nanomeshes using the self-assembled SiO_2@polymer composites. The best-performing catalyst showed STY(C_3H_6) of 0.72 $kg_{C3H6}{\cdot}kg_{cat}^{-1}{\cdot}h^{-1}$ and propene selectivity of 95% at 550 °C.[27] No information about catalyst durability was provided.

A common strategy to improve the efficiency of metal/metal-oxide supported catalysts is their modification with other metal/metal-oxide promoters.[14,28−32] Magnesium (Mg), an inexpensive and naturally abundant metal, was applied for this purpose.[33−36] For instance, the dispersion of VO_x species on the surface of Al_2O_3 could be increased by modifying the catalysts with magnesium, which was valuable for hindering coke formation.[36] Chu et al. also found that the use of Mg-doped SBA-15 support for Pt and SnO_x species is advantageous to increase their dispersion and to facilitate the transfer of coke species from the active sites to the support.[4] Liu et al. synthesized Co/MgS-1 catalysts via ion exchange for CO_2-assisted PDH, using MgS-1 support prepared through one-pot acid hydrolysis.[37] Ultrasmall $(CoO)_x$ clusters were anchored to the ion exchange sites of skeletal Mg^{2+}, forming an $Mg{-}(O{-}Co)_x$ structure active in this reaction. Our group also constructed MgO-modified ZnO_x/S-1 catalysts using a one-pot hydrothermal method, where a strong interaction between Mg^{2+} and ZnO_x stabilizes Zn^{2+} active sites, preventing their reduction to metallic Zn^0.[38]

Driven by the developments and challenges discussed above, Mg was selected as a promoter to regulate the redox, acidic, and structural properties of isolated CoO_x species in S-1, with the aim of elucidating their effects on PDH performance. The prepared catalysts were characterized using a range of complementary techniques including X-ray absorption, X-ray photoelectron, and ultraviolet-visible spectroscopy as well as temperature-programmed reduction with hydrogen, temperature-programmed desorption of ammonia or propene and X-ray diffraction. Pulse experiments involving C_3H_8 and C_3H_6, followed by pulsing O_2, were instrumental in analyzing the initial stages of cracking and coke formation reactions. The results obtained revealed that the Mg promoter favors the isolation of CoO_x by forming Co−O−Mg structures, which are characterized by lower reducibility and acidity strength than Co−O−Co or Co−O−Si structures. These changes are highly substantial, as they enhance the intrinsic PDH activity of the active Co-containing sites while suppressing the cracking and deep dehydrogenation reactions of propane and propene. Thus, we identified the fundamental reasons for controlling product selectivity in the PDH reaction. This information can be used to design efficient PDH catalysts that are not solely cobalt-based.

EXPERIMENTAL METHODS

Catalyst Synthesis

Silicalite-1 (S-1) was synthesized according to our previous work but with some modifications.[39] Firstly, TEOS (Sigma-Aldrich), TPAOH (1 M in water, Thermo Scientific) and deionized water were mixed with a molar ratio of TEOS:TPAOH:H_2O = 1:0.2:15 and stirred at room temperature for 6 h. The resulting clear solution was then transferred into a stainless-steel autoclave and subjected to hydrothermal treatment at 100 °C for 48 h. After cooling to room temperature, the solid material was collected by centrifugation, washed with deionized water five times, and finally calcined in air at 550 °C for 6 h to obtain the S-1 support.

A series of Co-containing catalysts with 2 wt% cobalt and different Mg amounts (0 to 4 wt%) were prepared by incipient wetness impregnation. First, a certain amount of S-1 was impregnated with an aqueous solution of $Co(NO_3)_2{\cdot}6H_2O$ (99%, Sigma-Aldrich) and $Mg(NO_3)_2{\cdot}6H_2O$ (99%, Fluka), and the resulting mixture was subsequently allowed to stand overnight. After that, the solids were dried at 100 °C for 12 h and then calcined in air at 550 °C for 2 h. The obtained samples were named as 2Co*x*Mg/S-1, where "*x*" stands for the weight percentage magnesium loading. The corresponding Co-free *x*Mg/S-1 samples were synthesized via the same procedure as that of 2Co*x*Mg/S-1 without adding $Co(NO_3)_2{\cdot}6H_2O$.

Catalyst Characterization

X-ray diffraction (XRD) patterns of the as-prepared samples were recorded on a Panalytical X'Pert θ/2θ-diffractometer equipped with Xcelerator detector using automatic divergence slits and Cu $k_{\alpha1}/_{\alpha2}$ radiation (40 kV, 40 mA, λ = 0.15406 nm, 0.15444 nm). Cu beta-radiation was excluded using a nickel filter.

UV-vis spectroscopic measurements of all samples were carried out using an Avantes spectrometer (AvaSpec-2048-USB2-RM) equipped with a high-temperature reflection UV-vis probe, an Ava-Light-DH-S-BAL deuterium-halogen light source and a CCD array detector. $BaSO_4$ (99.998%, Aldrich) was used as a white standard. The spectra were recorded at room temperature in the range of 200−1100 nm.

High angle angular dark-field scanning transmission electron microscopy (HAADF-STEM) tests were conducted on FEI Talos 200X with a working voltage of 200 kV. The aberration-corrected scanning transmission electron microscopy (AC-STEM) tests were carried out using FEI Titan Cubed Themis G2 300 operated at 300 kV to identify the microstructure and element distribution of the prepared catalysts.

Temperature-programmed reduction with hydrogen (H_2-TPR), temperature-programmed desorption of ammonia (NH_3-TPD), and temperature-programmed desorption of propene followed by oxygen temperature-programmed oxidation (C_3H_6-TPD/O_2-TPO) tests were carried out using an in-house developed setup containing eight individually heated continuous-flow fixed-bed quartz reactors. 50 mg (for H_2-TPR and C_3H_6-TPD/O_2-TPO) or 100 mg (for NH_3-TPD) of each catalyst was initially pretreated in a flow (10 mL·min^{-1}) of air (for H_2-TPR) or argon (for C_3H_6-TPD/O_2-TPO and NH_3-TPD) at 500 °C for 30 or 60 min. Hereafter, the treated catalysts were cooled to 100 °C (for H_2-TPR) or 50 °C (for C_3H_6-TPD/O_2-TPO and NH_3-TPD) in Ar. Hereafter, the temperature was ramped from 100 to 900 °C in a flow (10 mL·min^{-1}) of 5 vol% H_2 in Ar in H_2-TPR tests. For NH_3-TPD or C_3H_6-TPD/O_2-TPO tests, the treated catalysts were exposed to a flow of 1 vol% NH_3 in Ar (10 mL·min^{-1}) for 120 min and then purged with Ar for 6 h to remove physically adsorbed NH_3 or to a flow of 10 vol% C_3H_6 in Ar (6.25 mL·min^{-1}) for 120 min and then purged with Ar for 12 h to remove physically adsorbed C_3H_6 molecules. Finally, the reactors were heated from 50 to 600 °C in a flow of Ar with a heating rate of 10 °C·min^{-1}. After the C_3H_6 desorption experiments, the catalyst was again cooled to room temperature in Ar (10 mL·min^{-1}) followed by feeding 5 vol% O_2/Ar (10 mL·min^{-1}), and heating to 800 °C with a heating rate of 10 °C·min^{-1}. The signals at *m*/*z* of 2 (H_2), 16 (NH_2), 15 (NH), 18 (H_2O), 40 (Ar), 41 (C_3H_6), and 44 (CO_2) were recorded by an on-line mass spectrometer (Pfeiffer Vacuum OmniStar GSD 320).

X-ray photoelectron spectroscopy (XPS) analysis was performed on ESCALAB 220iXL (Thermo Fisher Scientific) equipped with monochromatic Al Kα radiation (*E* = 1486.6 eV). The electron binding energies were calibrated by charge compensation using a flood electron source and were referenced to the C 1s core level of adventitious carbon at 284.8 eV.

X-ray absorption spectroscopy (XAS) tests at the Co K-edge were carried out at the P65 beamline of PETRA III synchrotron radiation source (DESY, Hamburg) in transmission mode. Higher harmonics were rejected by a pair of Si plane mirrors installed in front of the monochromator. The energy of the X-ray photons was further selected

https://doi.org/10.1021/acscatal.6c01078
ACS Catal. 2026, 16, 8543−8554

by a Si(111) double-crystal monochromator and the beam size was set by means of slits to 0.4 (vertical) × 2.0 (horizontal) mm^2. The spectra were recorded in continuous mode while scanning incident energy from −150 to +800 eV relative to the respective absorption edge with a total time of 300 s and an integration time of 0.1 s. They were normalized, and the extended X-ray absorption fine structure spectra (EXAFS) background were subtracted using the ATHENA program from the IFEFIT software package.[40] The k^2-weighted EXAFS functions were Fourier transformed (FT) over the k range of 3.0−10.0 $Å^{-1}$ and multiplied by a Hanning window with a sill width of 1 $Å^{-1}$. The FT EXAFS spectra were not corrected for the phase shift. The fitting was performed in the *r*-space on k^1, k^2-weighted data in the *r*-range of 1.0−3.5 Å. Co foil as a reference compound was used to establish the value of the reduction factor S_0^2. For this purpose, the correlation between S_0^2 and the σ^2 was determined under different *k*-weightings ($k^n\chi(k)$, n = 0, 1, 2), which were obtained from modeling the first coordination sphere of Co foil. The crossing region of these curves was centered to obtain the value. This $S_0^2 = 0.78$ was fixed in the following refinement of the 2Co*x*Mg/S-1 atomic structure.

Diffuse reflectance infrared Fourier-transform spectroscopy (DRIFTS) measurements were carried out on the Bruker VERTEX 70 equipped with a ZnSe window. Typically, the catalysts were heated from room temperature to 500 °C in N_2 (10 mL·min^{-1}) and held for 30 min. The spectra were recorded with a resolution of 4 cm^{-1} from 600 to 4000 cm^{-1}.

N_2 adsorption-desorption isotherms were collected using a Belsorpmax II setup (Microtrac-BEL) at −196 °C. Prior to measurement, the catalysts were degassed under vacuum at 250 °C for 2 h. The specific surface area was calculated using the Brunauer−Emmett−Teller (BET) method, and the total pore volume was determined at a relative pressure (P/P_0) of 0.95.

The elemental composition (Co and Mg) of the as-prepared catalysts was determined by means of inductively coupled plasma optical emission spectrometry (ICP-OES) (Varian 715-ES).

C_3H_8- or C_3H_6-pulse experiments were performed at ambient pressure using 2Co/S-1 and 2Co1.6Mg/S-1 catalysts. Firstly, a 25 mg of sample was heated to 550 °C in a flow of He (20 mL·min^{-1}), and maintained at this temperature for 20 min. Subsequently, a C_3H_8/Ar = 1:19 mixture or a C_3H_6/Ar (1:19) mixture was pulsed 15 times with a pulse size of 1 mL to monitor the conversion of C_3H_8 or C_3H_6 and the formation of gaseous products. Thereafter, a 10 vol% O_2/Ar mixture was pulsed 10 times to oxidize the carbon deposits that had formed in the preceding C_3H_8 or C_3H_6 pulses. The signals at m/z of 44 (CO_2), 41 (C_3H_6), 40 (Ar), 32(O_2), 29 (C_3H_8), 28 (C_2H_x/CO, CO_2), 16 (CH_4), and 2 (H_2) were recorded by an on-line mass spectrometer (Pfeiffer Vacuum OmniStar GSD 350).

Catalytic Tests

Catalytic tests were performed using an in-house developed setup consisting of 15 continuous-flow fixed-bed quartz reactors. Typically, the catalyst (315−710 μm) was loaded in the middle of the reactor and then preheated to 550 °C in a N_2 flow with a heating rate of 10 °C·min^{-1}. Hereafter, a flow of 40 vol% C_3H_8/N_2 (10 mL·min^{-1}) was introduced.

To determine the apparent activation energy (E_a) of propene formation in the PDH reaction, catalytic tests were performed in the temperature range of 485−560 °C. The catalyst amount (10−30 mg) and the total flow rate (20−30 mL·min^{-1}) were varied to maintain propane conversion below 10%, ensuring differential reactor operation.

The durability of 2Co1.6Mg/S-1 was investigated in a series of five PDH/regeneration cycles at 550 °C, with a feed of 40 vol% C_3H_8 in N_2 at a total flow rate of 10 mL·min^{-1}. The catalyst amount was set to 100 mg. Each cycle consisted of: (i) propane dehydrogenation 60 min; (ii) purging with N_2 for 10 min; (iii) coke removal by calcination in air for 15 min at the same temperature; and (iv) flushing with N_2 (10 mL·min^{-1}) for 15 min.

An on-line gas chromatograph (Agilent 6890) equipped with PLOT/Q (for CO_2), AL/S (for hydrocarbons), and Molsieve 5 (for H_2, O_2, N_2 and CO) columns as well as flame ionization (FID) and thermal conductivity detectors (TCD) was used for quantifying the concentration of the feed components and reaction products.

The initial formation rate of propene ($r(C_3H_6)$), propane conversion ($X(C_3H_8)$), selectivity of gas-phase products (S_i) as well as the space time yield of propene formation ($STY(C_3H_6)$) were calculated using eqs 1−4, respectively.

$$r(C_3H_6) = \frac{\dot{n}^{out}_{C_3H_6}}{m_{cat}} \quad (1)$$

$$X(C_3H_8) = \frac{\dot{n}^{in}_{C_3H_8} - \dot{n}^{out}_{C_3H_8}}{\dot{n}^{in}_{C_3H_8}} \quad (2)$$

$$S_i = \frac{\nu_{C_3H_8}}{\nu_i} \times \frac{\dot{n}^{out}_i}{\dot{n}^{in}_{C_3H_8} - \dot{n}^{out}_{C_3H_8}} \quad (3)$$

$$STY_{(C_3H_6)} = \frac{F_{feed} \times \chi_{(C_3H_6)} \times M_{(C_3H_6)}}{1000 \times V_m \times m_{cat}} \quad (4)$$

$\dot{n}_i$ with superscripts in or out stands for the molar flows of gas-phase components at the reactor inlet or outlet. ν_i is the stoichiometric coefficient for product *i*. F_{feed} is the total feed flow. $\chi(C_3H_6)$ stands for the mole faction of propene at the reactor outlet, while m_{cat} is the mass of catalyst. N_2 was used as internal standard to consider reaction-induced changes in the number of moles.

RESULTS AND DISCUSSION

Platform of Catalysts and Their Physicochemical Characteristics

To understand the effect of the Mg promoter on the speciation and local coordination of CoO_x as well as its acidic and redox properties, in view of their relevance to the efficiency of propene formation in the PDH reaction, we prepared a series of 2Co*x*Mg/S-1 catalysts with *x* being 0, 0.2, 0.4, 1.6, 2.4, and 4 wt%. XRD analysis confirmed the structure of MFI zeolite in all samples (Figure 1a).[37,38] Based on the reflections in the 2θ range of 23°−25° (PDF#01-070-4743), only the orthorhombic MFI modification is present in all prepared samples (Figure S1a).[41] Any crystalline bulk Co- and/or Mg-containing phases were not identified in the obtained diffraction data (Figure 1a). It is worth noting that the reflections in the range of 7°−10° shifted to higher angles when the Mg content reached 4 wt% (Figure S1b). This suggests that a high Mg content may disrupt part of the MFI structure, leading to lattice contraction. Following the loading of Co and Mg, the specific surface area of the catalysts decreased but remained within the 400−500 $m^2 \cdot g^{-1}$ range, suggesting that high metal loading leads to a partial blockage of the pore in the zeolite framework (Figure S2 and Table S1).

Compared to the DRIFTS spectrum of bare S-1, the intensity of the band at 3550 cm^{-1}, associated with internal silanol nests, in the DRIFTS spectrum of 2Co/S-1 strongly decreased, while the band at 3740 cm^{-1}, corresponding to surface hydroxyl groups, decreased slightly (Figure S3).[42−44] This suggests that the silanol nests anchored CoO_x. The addition of the Mg promoter reduces the concentration of these defects further by consuming them for binding this promoter.

https://doi.org/10.1021/acscatal.6c01078
ACS Catal. 2026, 16, 8543−8554

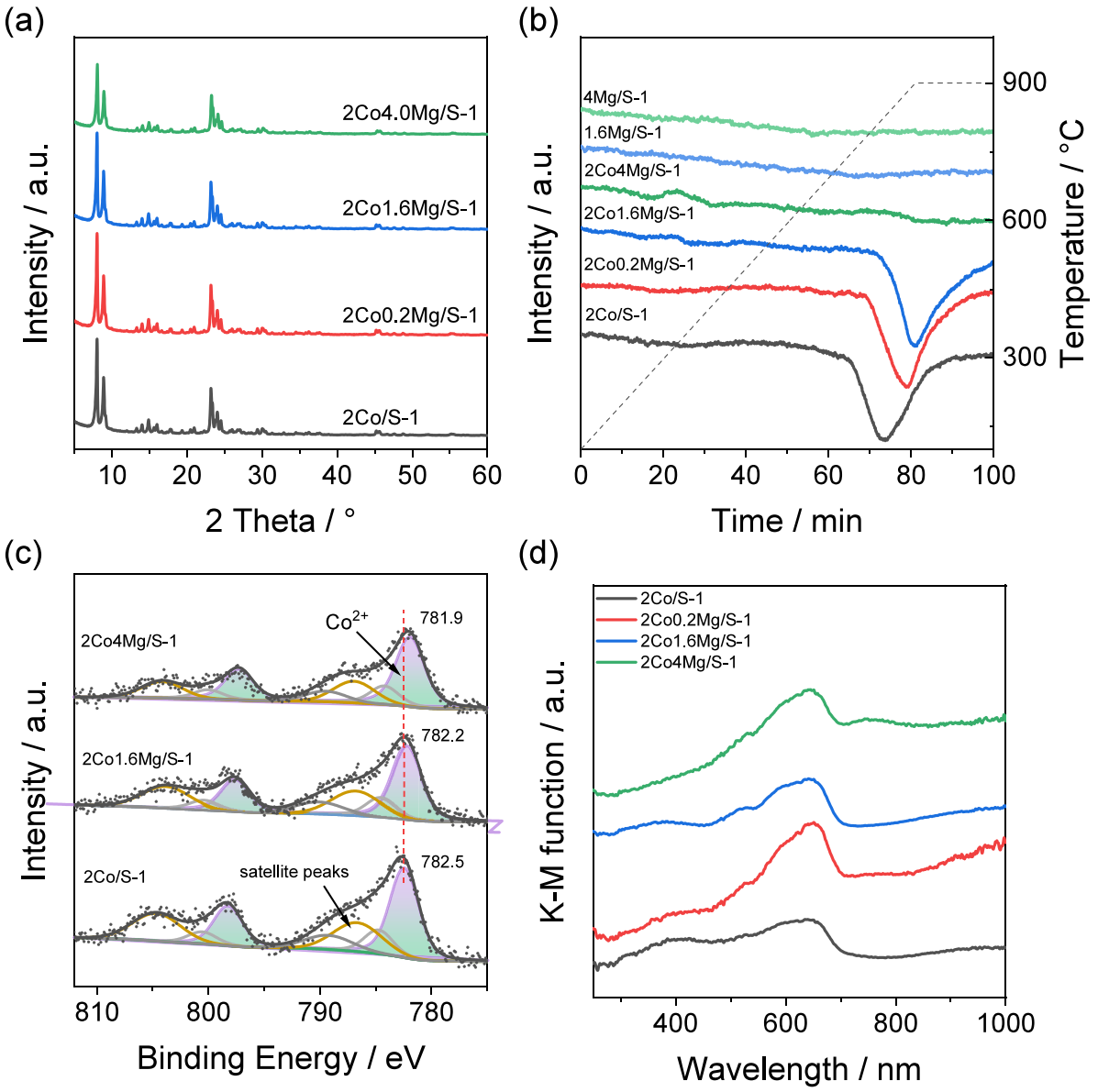

Figure 1. (a) XRD patterns, (b) H_2-TPR profiles, (c) XP, and (d) UV-vis spectra in the form of the Kubelka-Munk (K-M) function of as-prepared 2Co*x*Mg/S-1 catalysts (x = 0, 0.2, 1.6, and 4).

Only one H_2 consumption peak with the maximum at about 850 °C was identified in the H_2-TPR profile of 2Co/S-1 (Figure 1b), which is attributed to the reduction of CoO_x species that strongly interact with the S-1 support and should be highly dispersed.[20,45,46] Noticeably, the position of the maximum shifts to higher temperatures gradually as the Mg content increases from 0 to 1.6 wt%. The 2Co4Mg/S-1 and Co-free catalysts did not consume H_2 below 900 °C, the maximal temperature in our tests. Thus, the Mg promoter hinders the reducibility of the supported CoO_x species.

Two main XP signals at the binding energies (BEs) of approximately 782 and 798 eV are observed in the Co 2p region, see Figure 1c, which can be assigned to Co $2p_{3/2}$ and Co $2p_{1/2}$, respectively.[47,48] Furthermore, the presence of characteristic satellite peaks around 786.6 eV and 803.6 eV indicates that cobalt exists predominantly in the Co^{2+} state. Compared to the 2Co/S-1 sample, the Co $2p_{3/2}$ and Co $2p_{1/2}$ BEs of 2Co1.6Mg/S-1 and 2Co4Mg/S-1 are shifted to slightly lower values. This shift suggests an electronic interaction between Co^{2+} and Mg^{2+} species.

The presence of Co^{2+} species in all catalysts was further supported by UV-vis spectroscopy analysis (Figure 1d). The UV-vis spectra are characterized by bands at about 520, 590, and 645 nm, which can be attributed to the $^4T_{1g} \rightarrow {}^4T_{1g}(P)$ and $^4A_2 \rightarrow {}^4T_1(P)$ transitions of tetrahedral Co^{2+} species.[25,43,45,47]

Although the above results enabled us to conclude that Mg and Co are in close proximity to each other and interact strongly, we conducted an X-ray absorption analysis to gain a deeper understanding of the local structure of the CoO_x species. The XANES spectra of the 2Co/S-1, 2Co1.6Mg/S-1, and 2Co4Mg/S-1 catalysts are different from the reference spectra of Co foil, CoO and Co_3O_4 and characterized by the pre-edge peak at 7709.4 eV and the white line at 7725 eV (Figure 2a). The pre-edge feature at 7709−7710 eV is characteristic of

https://doi.org/10.1021/acscatal.6c01078
ACS Catal. 2026, 16, 8543−8554

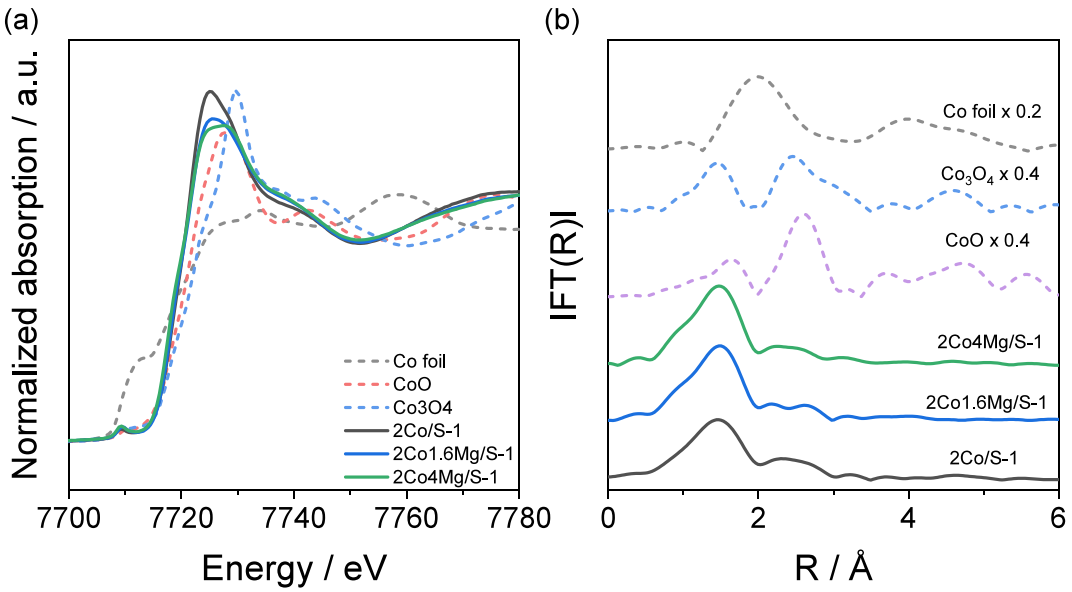

Figure 2. (a) XANES and (b) EXAFS spectra of 2Co/S-1, 2Co1.6Mg/S-1, and 2Co4Mg/S-1 as well as the reference samples (Co foil, CoO, and Co_3O_4) at the Co K-edge.

Co^{2+} and associated with the 1s → 3d excitation of low-spin Co species.[25,43,48] Thus, the oxidation state of Co in all catalysts should be +2, which is consistent with the XPS results. Moreover, the different white-line intensities at 7725 eV in the spectra of 2Co/S-1, 2Co1.6Mg/S-1 and 2Co4Mg/S-1 compared with the CoO and Co_3O_4 references indicate distinct local coordination environments, similar to those observed in Co-based catalysts with isolated Co^{2+} species.[24,25] However, introducing Mg into the catalyst (2Co1.6Mg/S-1 and 2Co4Mg/S-1) resulted in a decrease in the white line intensity compared to 2Co/S-1 suggesting that the electronic structure of CoO_x species is regulated by the promoter located in proximity in agreement with XPS data in Figure 1c.

Fourier-transform (FT) k^2-weighted extended X-ray absorption fine structure (EXAFS) analysis provided further insight into the differences in the local structure of the CoO_x species (Figure 2b). Regardless of the presence of Mg, a noticeable signal is present at about 1.5 Å, typical for the first shell Co−O scattering, while additional signals possibly originate from the second shell scattering paths.[24,47] The detailed EXAFS fitting parameters are listed in Table S2, and the corresponding fits are shown in Figure S4. Based on the average coordination numbers (CNs) for the Co−O and Co−(O)−Co paths of 5.1 and 0.7, respectively, the 2Co/S-1 sample contains highly dispersed CoO_x species, most of which are isolated. In addition, the presence of Co−O−Si bonds evidences a strong interaction between the CoO_x species and the S-1 support. For the 2Co1.6Mg/S-1 and 2Co4Mg/S-1 catalysts, the Co−O CNs of 5.3/5.2 and the absence of a Co−O−Co bond indicate that Co^{2+} is atomically dispersed. Based on high angle angular dark-field scanning transmission electron microscopy (AC-HAADF-STEM) analysis, cobalt on the surface of 2Co1.6Mg/S-1 should be atomically dispersed (Figure S5). In addition, long-range scattering associated with Co−O−Si or Co−O−Mg bonds was detected. The CNs of these higher-shell contributions increased from 1.0 to 1.8 as the Mg content increased from 1.6 to 4 wt%. However, these two scattering paths cannot be distinguished by EXAFS (Table S2). Combined with the XPS and TPR results, the data supports the presence of a local interaction between the Co^{2+} center and Mg^{2+} promoter.

Catalytic Performance

The initial (after 5 min on propane stream) rate of propene formation determined at 550 °C over the 2Co*x*Mg/S-1 catalysts passes a maximum with increasing Mg loading reaching its highest value of 1.6 mmol·g^{-1}·min^{-1} at 1.6 wt% Mg (Figure 3a). This catalyst has lower apparent activation energy of propene formation compared to 2Co/S-1, i.e., 75 kJ·mol^{-1} versus 96 kJ·mol^{-1} (Figure 3b), suggesting the positive Mg effect on the intrinsic activity of highly dispersed CoO_x. As the Co-free 1.6Mg/S-1 and 4Mg/S-1 catalysts are nearly inactive (Figure S6), the negative effect of the promoter on the rate of propene formation at Mg loadings above 1.6 wt% can be due to the coverage of the active CoO_x sites by the promoter in view of the XPS data in Table S3. The effect of other alkali or alkaline earth metal promoters (1.6 wt%) on the PDH activity of the 2Co/S-1s catalyst was also investigated. The former promoters led to a decrease in the rate of propene formation (Figure S7a). Alkaline earth metal promoters exhibited an enhancing effect, with the most pronounced one being caused by Mg (Figure S7b).

We also tested the 2Co*x*Mg/S-1 catalysts under industrially relevant degrees of propane conversion at a weight hourly space velocity (WHSV) of 4.7 h^{-1} (Figure 3c,d). The 2Co/S-1 catalyst showed an initial (after 5 min on stream) propane conversion of 28.7%, which dropped to 20.9% after the next 5 min on stream followed by a decrease to about 11.9% after 250 min on stream. The selectivity to propene increased from 25.1 to 95.7%, respectively. Based on the low initial propene selectivity, it can be concluded that the initial propane conversion is primarily attributed to side reactions rather than to dehydrogenation. The initial selectivity to propene increases with increasing magnesium loading, without any obvious negative

https://doi.org/10.1021/acscatal.6c01078
ACS Catal. 2026, 16, 8543−8554

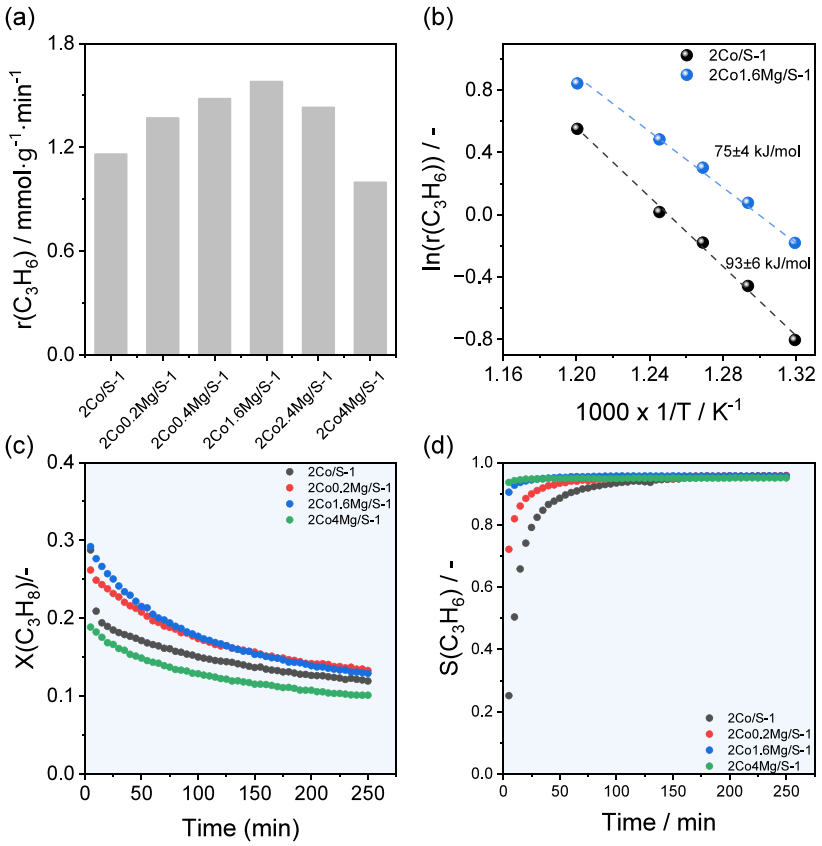

Figure 3. (a) Initial propene formation rate over 2Co*x*Mg/S-1 samples (x = 0, 0.2, 0.4, 1.6, 2.4, and 4). Reaction conditions: T = 550 °C, catalyst amount = 25 mg, WHSV (C_3H_8) = 34.4 h^{-1}, C_3H_8:N_2 = 2:3. (b) Arrhenius plots of the propene formation rate over 2Co/S-1 and 2Co1.6Mg/S-1 as well as the respective apparent activation energy (E_a). Time-on-stream profiles of (c) propane conversion and (d) propene selectivity over 2Co*x*Mg/S-1 catalysts (x = 0, 0.2, 1.6, and 4). Reaction conditions: T = 550 °C, C_3H_8:N_2 = 2:3, WHSV(C_3H_8) = 4.7 h^{-1}.

effect on the initial propane conversion at Mg loadings below 4 wt%. This result suggests that the promoter hinders side reactions in favor of propene formation (Figure 3d). The highest initial propane conversion of 29.2% was obtained over 2Co1.6Mg/S-1, with a propene selectivity of 90.5%. Spent 2Co/S-1 and 2Co1.6Mg/S-1 catalysts after 250 min propane stream were characterized by temperature-programmed oxidation tests with O_2 (Figure S8). A lower coke content was found for the 2Co1.6Mg/S-1 catalyst although it showed higher propane conversion in the preceding PDH tests, suggesting its lower ability to form coke deposits.

The most promising 2Co1.6Mg/S-1 catalyst was also tested with an analogue of commercial K-CrO_x/Al_2O_3 catalyst in parallel to directly compare their performance. Our catalyst outperformed the reference catalyst in terms of propane conversion and space time yield of propene formation (STY (C_3H_6)) at slightly lower initial propene selectivity throughout the entire testing period (Figures 4a and S9). We also benchmarked the 2Co1.6Mg/S-1 catalyst against previously reported Co-based catalysts regarding propene productivity. For a proper comparison of the catalysts tested under different reaction conditions, the STY (C_3H_6) values were plotted versus the ratio of the experimentally measured propane conversion to the corresponding equilibrium one ($X(C_3H_8)_{exp}/X(C_3H_8)_{eq}$). In general, industrially relevant catalysts are expected to show high productivity at $X(C_3H_8)_{exp}/X(C_3H_8)_{eq}$ values approaching unity. Our catalyst achieved the initial STY(C_3H_6) value of 1.2 $kg_{C3H6}{\cdot}kg_{cat}^{-1}{\cdot}h^{-1}$ at 550 °C and 68% equilibrium propane conversion, outperforming most previously reported catalysts even tested at higher temperatures (Figure 4b and Table S4).

Finally, the durability of the 2Co1.6Mg/S-1 catalyst was demonstrated in a series of five dehydrogenation/regeneration cycles (Figure 4c). The PDH (40 vol% C_3H_8 in N_2) and regeneration (20 vol% O_2 in N_2) cycles lasted 60 min and 15 min, respectively, at the same temperature (550 °C). In each PDH cycle, the propane conversion gradually decreased due to the accumulation of coke, while the selectivity to propene increased. The initial conversion could be restored to a major extent after removing coke by simple catalyst calcination in air. The high productivity and durability of the 2Co1.6Mg/S-1 catalyst developed in the present work further emphasizes the commercial application potential of Co-based catalysts for PDH. The spent 2Co1.6Mg/S-1 catalyst after five PDH/regeneration cycles was characterized by HRTEM, XRD and UV-Vis (Figures S10 and S11). The results obtained show that the catalyst structure did not change proving its durability.

Origins of the Mg Enhancing Effect on the Performance of Co/S-1 Catalysts in PDH

Based on our complementary characterization study (Figures 1, 2, S4, and Table S2), we are confident that the promoter Mg helps to form isolated CoO_x species by forming strong Co−O−Mg bonds. Such species exhibit higher intrinsic activity than CoO_x bound to S-1 only via Co−O−Si bonds due to

https://doi.org/10.1021/acscatal.6c01078
ACS Catal. 2026, 16, 8543−8554

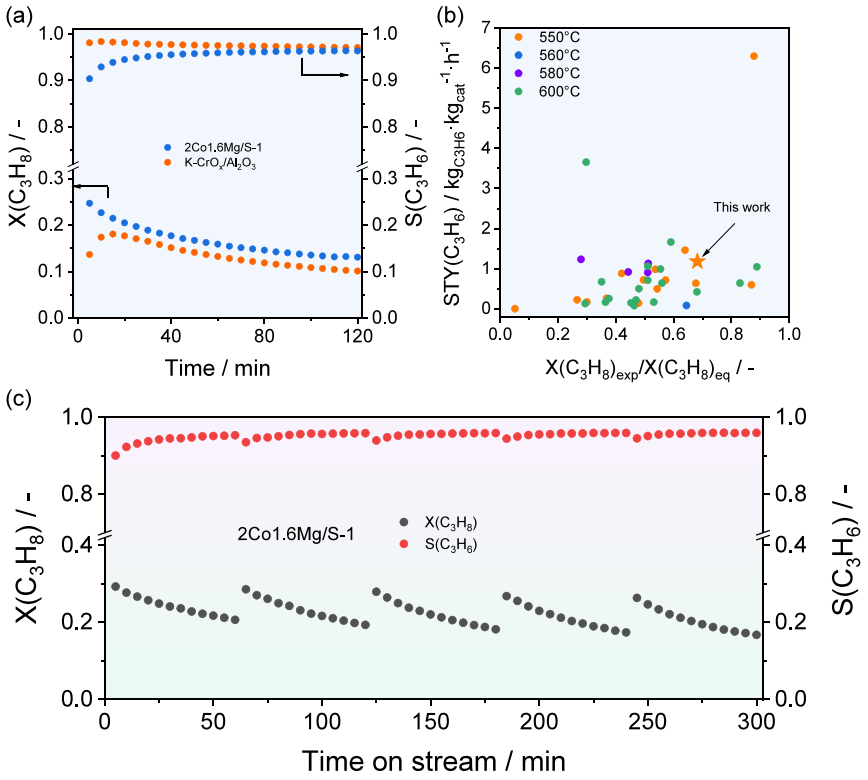

Figure 4. (a) Time-on-stream profiles of propane conversion ($X(C_3H_8)$) and propene selectivity ($S(C_3H_6)$) obtained in PDH over 2Co1.6Mg/S-1 and K-CrO_x/Al_2O_3. Reaction conditions: T = 550 °C, C_3H_8:N_2 = 2:3, WHSV(C_3H_8) = 9.4 h^{-1}. (b) STY(C_3H_6) determined over 2Co1.6Mg/S-1 and previously reported Co-based catalysts (Table S4) at different temperatures versus $X(C_3H_8)_{exp}/X(C_3H_8)_{eq}$. (c) $X(C_3H_8)$ and $S(C_3H_6)$ over 2Co1.6Mg/S-1 in five PDH/regeneration cycles. Reaction conditions: T = 550°C, C_3H_8:N_2 = 2:3, WHSV(C_3H_8) = 4.7 h^{-1}, catalyst amount = 100 mg. Each cycle consisted of a PDH stage lasted for 60 min and a regeneration stage lasted for 15 min.

lowering the activation energy for propene formation (Figure 3b). A high Mg loading is disadvantageous because there is a possibility that the active CoO_x species will be covered by excess promoter, resulting in a decrease in the overall catalyst activity.

To understand the effect of the Mg promoter on product selectivity, we performed a series of catalytic tests at different WHSV to achieve various degrees of propane conversion for analyzing how the selectivity to C_3H_6, cracking products (CH_4, and C_2H_x) and coke changes (Figure 5). For the 2Co/S-1 catalyst, the selectivity to these products extrapolated to zero propane conversion is about 91, 3, and 6%, respectively (Figure S12). Thus, all these products can be formed directly from propane but with different rates according to the following order C_3H_6 >> cracking products > coke. In contrast, the selectivity of the Mg-modified catalysts to propene extrapolated to zero propane conversion is almost 100%. Thus, the promoter inhibited the direct conversion of propane to cracking products

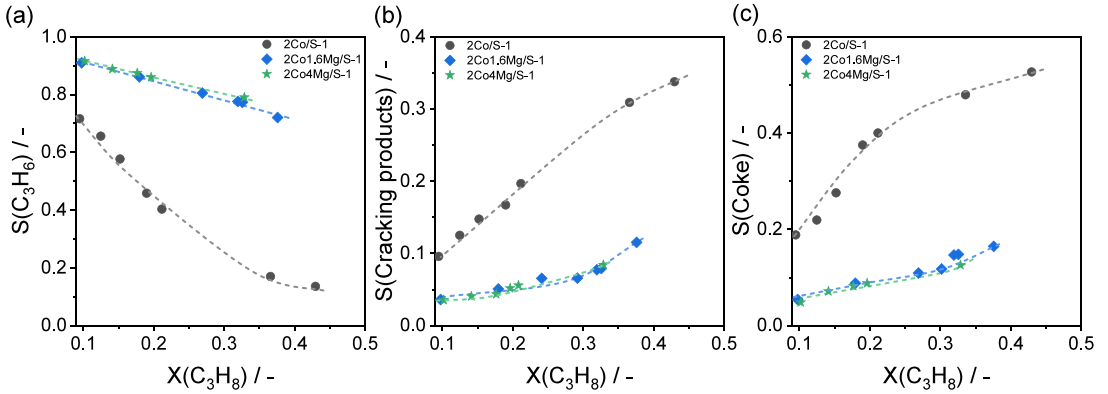

Figure 5. Selectivity-conversion relationships for (a) propene, (b) cracking products (C_1−C_2 hydrocarbons), and (c) coke formed over 2Co*x*Mg/S-1 samples (x = 0, 1.6, and 4).

https://doi.org/10.1021/acscatal.6c01078
ACS Catal. 2026, 16, 8543−8554

and coke while maintaining high activity in the formation of propene, which is the only product formed directly from propane. In addition, the promoter reduced the rates of propene conversion to coke and cracking products as reflected by the slope of the selectivity-conversion relationships for these products (Figure 5). The higher the slope, the higher the rates are. In this regard, the catalysts can be ordered as follows: 2Co/S-1 >> 2Co1.6Mg/S-1 ≥ 2Co4Mg/S-1.

C_3H_8-pulse experiments were conducted to gain insight into the reaction pathway at the initial reaction stage at low propane concentration. Propane conversion over 2Co/S-1 passed a maximum with increasing number of propane pulses and was significantly higher compared to 2Co1.6Mg/S-1 (Figure S13). As the former catalyst produced significant amounts of propene only during the first 4 pulses, while C_2-hydrocarbons and CH_4 were formed in all pulses, the latter two products must have been formed from propane, but not from propene (Figure 6a). The amount of CH_4 additionally increased from pulse to pulse. In contrast to 2Co/S-1, 2Co1.6Mg/S-1 selectively converted propane to propene in all pulses and produced low amounts of C_2-hydrocarbons and CH_4, demonstrating the limited ability of CoO_x species interacting with Mg to crack propane (Figure 6b). O_2 pulse experiments performed after the C_3H_8-pulse experiments revealed that the coke content determined in the latter tests on 2Co/S-1 was approximately 32 times higher than that on 2Co1.6Mg/S-1 (Figures 6c and S14).

Further C_3H_6-pulse experiments confirmed the positive role of Mg in hindering the conversion of this olefin to CH_4 and C_2-hydrocarbons (Figure 6d,e). The coke content was also quantified by O_2 pulse experiments after 15 consecutive propene pulses. The result was approximately twice as high for 2Co/S-1 as for 2Co1.6Mg/S-1 (Figures 6f and S15), suggesting that the promoter also inhibits the ability of CoO_x species to catalyze propene deep dehydrogenation.

Based on the above discussion, it can be concluded that the promoter Mg inhibits the cracking of propane and propene as

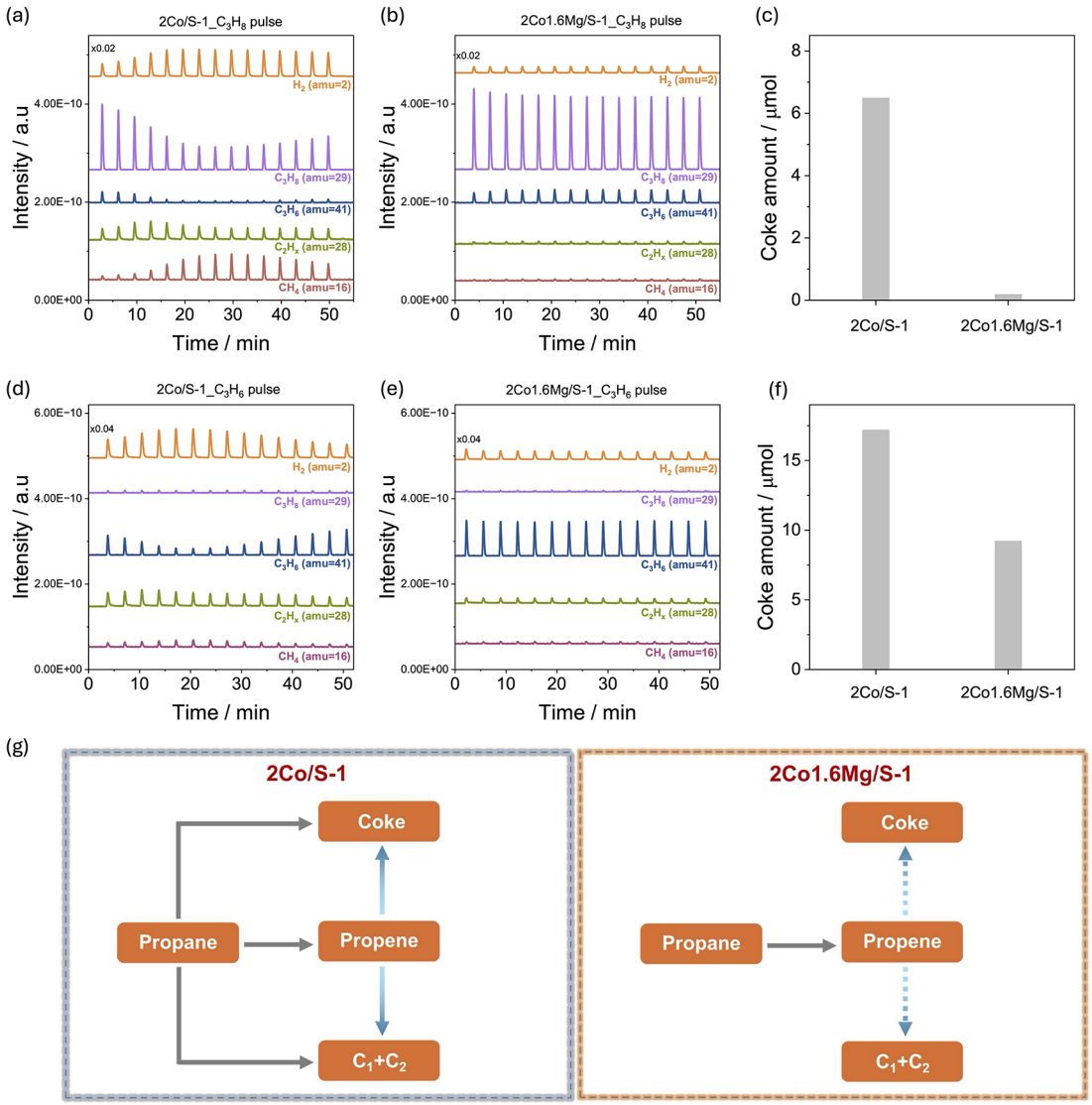

Figure 6. Responses of the reaction products formed over (a, d) 2Co/S-1 and (b, e) 2Co1.6Mg/S-1 in (a, b) C_3H_8-pulse tests (C_3H_8:Ar = 1:19, 1mL pulse size) or (d, e) C_3H_6-pulse tests (C_3H_6:Ar = 1:19, 1mL pulse size) at 550 °C. The amount of coke formed in O_2-pulse tests (O_2:Ar = 1:9, 1mL pulse size) performed at 550 °C after the (c) C_3H_8- and (f) C_3H_6-pulse tests in (a, b) and (d, e), respectively. (g) Proposed reaction pathways of the formation of products in propane dehydrogenation.

https://doi.org/10.1021/acscatal.6c01078
ACS Catal. 2026, 16, 8543−8554

well as the deep dehydrogenation of propene. As a consequence, propene selectivity improves. Accordingly, the role of Mg in controlling product formation in the PDH reaction is schematically proposed in Figure 6g.

Catalyst acidity is usually considered to be one of the key factors that regulate product selectivity, particularly with regard to the formation of coke.[49−51] To check if these considerations are also applicable to the present materials with and without Mg, we performed NH_3-TPD tests (Figure 7a). Given that both Mg^{2+} and Co^{2+} act as Lewis's acid sites capable of interacting with NH_3, we subtracted the obtained NH_3 profiles of the *x*Mg/S-1 materials from those of their counterparts containing Co, i.e., 2Co*x*Mg/S-1, to consider the influence of Mg on acidic properties of CoO_x in comparison with unpromoted 2Co/S-1. Two regions of NH_3 desorption were identified with the maximal rates below 200 °C and above 300 °C (Figure 7b). They can be assigned to the presence of weak acidic and strong acidic CoO_x sites, respectively.[52−55] Integrating the NH_3 desorption profiles using two Gaussian functions revealed that the concentration of the strong acidic sites decreased significantly after introducing Mg, while the concentration of the weak acidic sites increased and reached its highest value for the 2Co1.6Mg/S-1 catalyst (Figure 7b and Table S5). The strong CoO_x acidic sites play an important for achieving high propene selectivity under industrially relevant conditions; the lower their concentration, the higher the selectivity (Figure 7c). Contrarily, weak acidic CoO_x sites appear to be efficient for propene productivity (Figure 7d). Thus, introducing an appropriate amount of Mg into the Co/S-1 catalyst modulates the acidity of the CoO_x species through direct Co−O−Mg interactions. This decreases the concentration of CoO_x-related strong acid sites associated with side reactions (such as cracking and deep dehydrogenation), while increasing the number of Co-related weak acid sites that favor propene formation. This enhances both propene selectivity and productivity.

C_3H_6-TPD tests/O_2-TPO tests provided further insights into the role of Mg in enhancing propene selectivity. In these tests, propene was initially adsorbed at 50 °C followed by a temperature-programmed desorption step up to 600 °C, cooling to room temperature in Ar followed by a TPO step up to 800 °C. Whereas propene desorbed from 2Co1.6Mg/S-1 and 2Co4Mg/S-1, no propene desorption was observed in the C_3H_6-TPD tests with 2Co/S-1 and 2Co0.2Mg/S-1 (Figure 7e). However, CO_2 was formed in the subsequent TPO step (Figure 7f), indicating the presence of strongly adsorbed propene species, which did not desorb in the preceding C_3H_6-TPD step, but were oxidized. Based on these results we suggest that the concentration of sites weakly adsorbing C_3H_6 can be determined from the amount of propene desorbed in the C_3H_6-TPD step, while the amount of CO_2 formed in the TPO step represents the concentration of sites strongly adsorbing C_3H_6. The concentration of the former sites increases with increasing Mg content reaching its maximum value at 2Co1.6Mg/S-1, before decreasing (Figure 7g). A similar volcano-shaped trend was found for the initial propene formation rate, indicating the key role of weak propene adsorption sites for the efficient propane dehydrogenation to the desired product. In contrast, the space-time yield of coke formation increases with the number of strong propene adsorption sites (2Co4Mg/S-1 < 2Co1.6Mg/S-1 < 2Co0.2Mg/S-1 < 2Co/S-1)

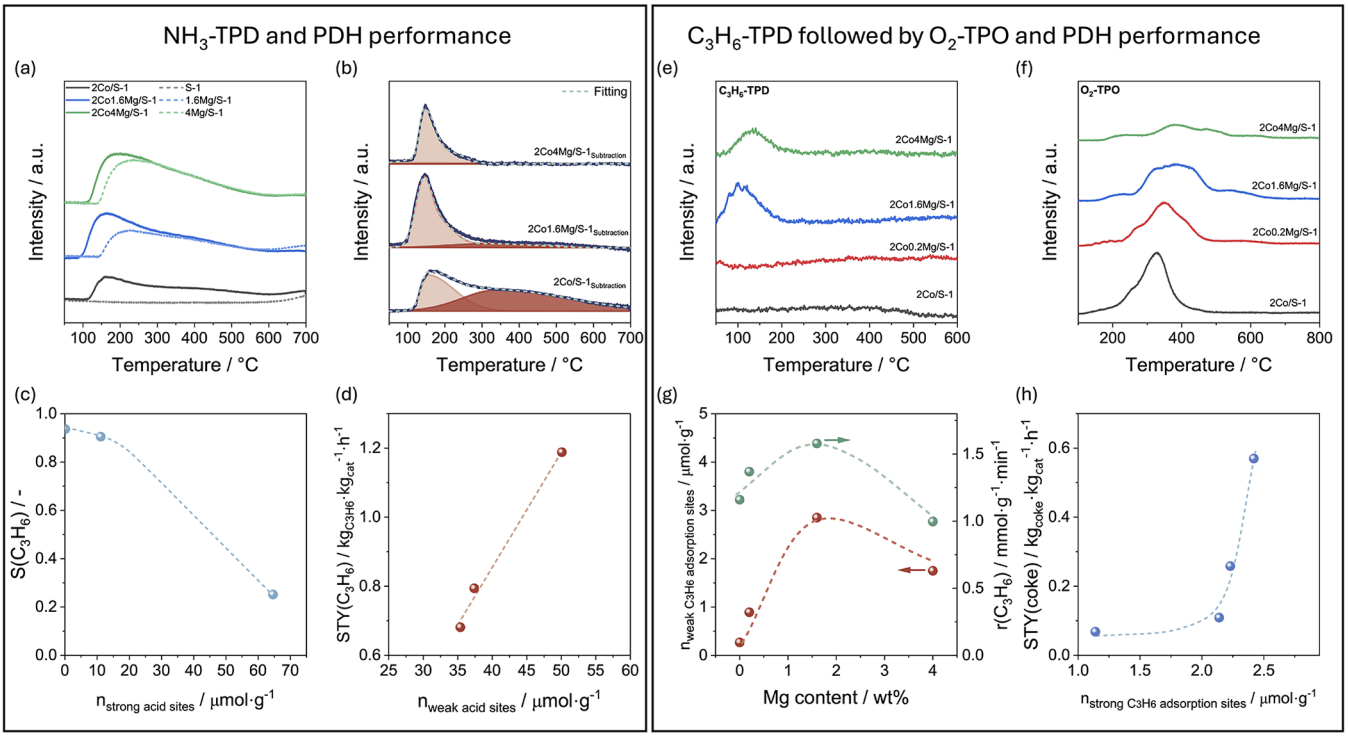

Figure 7. (a) NH_3-TPD profiles of 2Co*x*Mg/S-1 ($x = 0$, 1.6, and 4) and Co-free *x*Mg/S-1 samples. (b) Desorption profiles of NH_3 related to CoO_x sites as calculated from the profiles in (a). (c) Initial $S(C_3H_6)$ from Figure 3d versus the amount of strong acid sites calculated from the dark brown area in (b). (d) $STY(C_3H_6)$ versus the amount of weak acid sites from the light brown area in (b). (e) C_3H_6-TPD and (f) O_2-TPO profiles of 2Co*x*Mg/S-1. (g) Concentration of propene (C_3H_6) weak adsorption sites calculated from (e) and the initial $r(C_3H_6)$ versus the Mg content of in 2Co*x*Mg/S-1. (h) Initial STY (coke) versus the amount of propene (C_3H_6) strong adsorption sites calculated from (f).

https://doi.org/10.1021/acscatal.6c01078
ACS Catal. 2026, 16, 8543−8554

(Figure 7h). This observation suggests that these sites play a key role in coke formation in the PDH reaction and are consequently responsible for propene loss as propane conversion increases.

CONCLUSIONS

In this study, we performed a comprehensive kinetic and material characterization analysis aimed at understanding how to control catalyst activity and propene selectivity in the PDH reaction, using the Co-Silicalite-1 system prepared by an industrially relevant method as an example. This analysis revealed that the introduction of Mg as a promoter into this system enables the regulation of the local structure and dispersion of CoO_x species, with these characteristics influencing the acidic and redox properties of the supported species. The promoter decreases the strength of the Co-related acidic sites and hinders the reductivity of CoO_x species due to the formation of Co−O−Mg structures. Such species perform superior to those with Co−O−Co or Co−O−Si bonds in terms of PDH activity and propene selectivity. As evidenced by pulse experiments involving C_3H_8 and C_3H_6, followed by pulsing O_2 and catalytic tests in a broad range of propane conversion, the Mg promoter suppresses both cracking and deep dehydrogenation reactions of propane/propene, thereby enabling propene selectivity above 90% at propane conversion of about 70% of the equilibrium conversion. The obtained results highlight the critical importance of controlling the local structure of highly dispersed CoO_x for the rational design of high-performance Co-based catalyst for PDH under industrial conditions.

ASSOCIATED CONTENT

Supporting Information

The Supporting Information is available free of charge at https://pubs.acs.org/doi/10.1021/acscatal.6c01078.

Catalyst characterization and performance results, including structural and morphological information (XRD patterns, TEM images, and N_2 adsorption−desorption isotherms), surface properties (DRIFTS), and CoO_x structural properties (UV−vis spectra and XAS fitting results), coke analysis (TPO), catalytic performance (PDH reaction, C_3H_8 pulse/O_2 pulse, and C_3H_6 pulse/O_2 pulse experiments), and comparison of catalytic performance among different catalysts (PDF)

AUTHOR INFORMATION

Corresponding Authors

Qiyang Zhang – *Leibniz-Institut für Katalyse e.V., Albert-Einstein-Str. 29a, Rostock, D-18059 Germany;* Email: Qiyang.Zhang@catalysis.de

Evgenii V. Kondratenko – *Leibniz-Institut für Katalyse e.V., Albert-Einstein-Str. 29a, Rostock, D-18059 Germany;* orcid.org/0000-0003-0431-6937; Email: Evgenii.kondratenko@catalysis.de

Authors

Xiangnong Ding – *Leibniz-Institut für Katalyse e.V., Albert-Einstein-Str. 29a, Rostock, D-18059 Germany*

Dmitry E. Doronkin – *Institute for Chemical Technology and Polymer Chemistry, and Institute of Catalysis Research and Technology, Karlsruhe Institute of Technology, Kaiserstr. 12, Karlsruhe, D-76131 Germany;* orcid.org/0000-0003-3930-3204

Stephan Bartling – *Leibniz-Institut für Katalyse e.V., Albert-Einstein-Str. 29a, Rostock, D-18059 Germany;* orcid.org/0000-0001-5901-7235

Henrik Lund – *Leibniz-Institut für Katalyse e.V., Albert-Einstein-Str. 29a, Rostock, D-18059 Germany;* orcid.org/0000-0001-7747-2178

Dongxu Wang – *Max Planck Institute of Microstructure Physics, Weinberg 2, Halle, 06120 Germany;* orcid.org/0009-0008-4410-8239

Elizaveta Fedorova – *Leibniz-Institut für Katalyse e.V., Albert-Einstein-Str. 29a, Rostock, D-18059 Germany*

Christoph Kubis – *Leibniz-Institut für Katalyse e.V., Albert-Einstein-Str. 29a, Rostock, D-18059 Germany;* orcid.org/0000-0001-9549-2455

Complete contact information is available at: https://pubs.acs.org/doi/10.1021/acscatal.6c01078

Author Contributions

The manuscript was written through contributions of all authors. All authors have given approval to the final version of the manuscript.

Notes

The authors declare no competing financial interest.

ACKNOWLEDGMENTS

Financial support by the State of Mecklenburg-Vorpommern is gratefully acknowledged. We acknowledge DESY (Hamburg, Germany), a member of the Helmholtz Association HGF, for the prevision of experimental facilities. Parts of this research were carried out at PETRA III, and we would like to thank Dr. Edmund Welter for assistance in using beamline P65. Beamtime was granted for the proposals I-20240852 and I-20250490.

REFERENCES

(1) Chen, S.; Chang, X.; Sun, G.; Zhang, T.; Xu, Y.; Wang, Y.; Pei, C.; Gong, J. Propane dehydrogenation: catalyst development, new chemistry, and emerging technologies. *Chem. Soc. Rev.* **2021**, *50* (5), 3315–3354.

(2) Dai, Y.; Gao, X.; Wang, Q.; Wan, X.; Zhou, C.; Yang, Y. Recent progress in heterogeneous metal and metal oxide catalysts for direct dehydrogenation of ethane and propane. *Chem. Soc. Rev.* **2021**, *50* (9), 5590–5630.

(3) Otroshchenko, T.; Jiang, G.; Kondratenko, V. A.; Rodemerck, U.; Kondratenko, E. V. Current status and perspectives in oxidative, non-oxidative and CO_2-mediated dehydrogenation of propane and isobutane over metal oxide catalysts. *Chem. Soc. Rev.* **2021**, *50* (1), 473–527.

(4) Li, B.; Xu, Z.; Jing, F.; Luo, S.; Chu, W. Facile one-pot synthesized ordered mesoporous Mg-SBA-15 supported PtSn catalysts for propane dehydrogenation. *Appl. Catal., A* **2017**, *533*, 17–27.

(5) Han, S.; Zhao, Y.; Otroshchenko, T.; Zhang, Y.; Zhao, D.; Lund, H.; Vuong, T. H.; Rabeah, J.; Bentrup, U.; Kondratenko, V. A.; et al. Unraveling the Origins of the Synergy Effect between ZrO_2 and CrO_x in Supported $CrZrO_x$ for Propene Formation in Nonoxidative Propane Dehydrogenation. *ACS Catal.* **2020**, *10* (2), 1575–1590.

(6) Han, S.; Zhao, D.; Otroshchenko, T.; Lund, H.; Bentrup, U.; Kondratenko, V. A.; Rockstroh, N.; Bartling, S.; Doronkin, D. E.; Grunwaldt, J.-D.; et al. Elucidating the Nature of Active Sites and Fundamentals for their Creation in Zn-Containing ZrO_2−Based

Catalysts for Nonoxidative Propane Dehydrogenation. *ACS Catal.* **2020**, *10* (15), 8933–8949.
(7) Zhao, D.; Tian, X.; Doronkin, D. E.; Han, S.; Kondratenko, V. A.; Grunwaldt, J.-D.; Perechodjuk, A.; Vuong, T. H.; Rabeah, J.; Eckelt, R.; et al. In situ formation of ZnO_x species for efficient propane dehydrogenation. *Nature* **2021**, *599* (7884), 234–238.
(8) Zhang, Q.; Li, Y.; Otroshchenko, T.; Kondratenko, V. A.; Wu, K.; Fedorova, E. A.; Doronkin, D. E.; Bartling, S.; Lund, H.; Jiang, G.; et al. The enhancing effect of Co^{2+} on propane non-oxidative dehydrogenation over supported Co/ZrO_2 catalysts. *J. Catal.* **2024**, *432*, No. 115440.
(9) Hong, H.; Xu, Z.; Mei, B.; Hu, W.; Fornasiero, P.; Wang, C.; Wang, T.; Yue, Y.; Li, T.; Yang, C.; et al. A self-regenerating Pt/Ge-MFI zeolite for propane dehydrogenation with high endurance. *Science* **2025**, *388* (6746), 497–502.
(10) Wu, K.; Kondratenko, V. A.; Zhou, M.; Doronkin, D. E.; Bartling, S.; Zhang, Q.; Han, S.; Jia, X.; Liu, Q.; Xiong, D.; et al. The Role of Reducibility of $PtGaO_x$-Based Catalysts for Efficient and Durable Propane Dehydrogenation. *Angew. Chem., Int. Ed.* **2025**, *64* (31), No. e202506704.
(11) Xu, Z.; Gao, M.; Wei, Y.; Yue, Y.; Bai, Z.; Yuan, P.; Fornasiero, P.; Basset, J.-M.; Mei, B.; Liu, Z.; et al. Pt migration−lockup in zeolite for stable propane dehydrogenation catalyst. *Nature* **2025**, *643* (8072), 691–698.
(12) Yang, M.; Fan, D.; Wei, Y.; Tian, P.; Liu, Z. Recent Progress in Methanol-to-Olefins (MTO) Catalysts. *Adv. Mater.* **2019**, *31* (50), No. 1902181.
(13) Sofi, M. H. M.; Hamid, M. Y. S.; Jalil, A. A.; Alhebshi, A.; Hassan, N. S.; Bahari, M. B.; Mohamud, M. Y. Recent Advancements of SAPO-34 and ZSM-5 Zeolite in Converting Methanol to Olefin: A Review. *Arab. J. Sci. Eng.* **2025**, *50* (6), 3671–3697.
(14) Motagamwala, A. H.; Almallahi, R.; Wortman, J.; Igenegbai, V. O.; Linic, S. Stable and selective catalysts for propane dehydrogenation operating at thermodynamic limit. *Science* **2021**, *373* (6551), 217–222.
(15) Zhang, Q.; Li, Y.; Tian, X.; Kondratenko, V. A.; Fedorova, E. A.; Yang, T.; Ding, X.; Doronkin, D. E.; Zhao, D.; Deng, C.; et al. Mixed-valence $Co^{0/II}O_x$ clusters on silicalite-1 facilitate propane dehydrogenation to propene. *Nat. Catal.* **2026**.
(16) Huang, Z.; He, D.; Deng, W.; Jin, G.; Li, K.; Luo, Y. Illustrating new understanding of adsorbed water on silica for inducing tetrahedral cobalt(II) for propane dehydrogenation. *Nat. Commun.* **2023**, *14* (1), 100.
(17) Yao, Y.; Wang, J.; Liu, Q.; Yu, C.; Gao, Z.; Yuan, F.; Wang, X. Improving the Selectivity and Stability of Supported Cobalt Catalysts via Static Bi-Doping and Dynamic Trace CO_2 Co-Feeding During Propane Dehydrogenation. *Angew. Chem., Int. Ed.* **2025**, *64* (3), No. e202415295.
(18) Liu, Q.; Yao, Y.; Li, J.; Wang, J.; Chen, L.; Li, W.; Guo, Y.; Yao, S.; Yang, Y.; Wang, X. Stable Cobalt−Zeolite Propane-Dehydrogenation Catalysts Enabled by Reaction-Driven Reconstruction. *Angew. Chem., Int. Ed.* **2025**, *64* (21), No. e202505628.
(19) Zhang, Q.; Kondratenko, V. A.; Ding, X.; Weiss, J.; Bartling, S.; Fedorova, E.; Zhao, D.; Doronkin, D. E.; Wang, D.; Kubis, C.; et al. Understanding the reaction-induced restructuring of CoO_x species in silicalite-1 to control selectivity in non-oxidative dehydrogenation of propane. *Chin. J. Catal.* **2025**, *74*, 108–119.
(20) Zhou, H.; Li, H.; Wang, L.; Chu, S.; Liu, L.; Liu, L.; Qi, J.; Ren, Z.; Cai, A.; Hui, Y.; et al. Cobaltosilicate zeolite beyond platinum catalysts for propane dehydrogenation. *Nat. Catal.* **2025**, *8* (4), 357–367.
(21) Zhang, Q.; Zhang, T.; Liu, B.; Fedorova, E.; Doronkin, D. E.; Kondratenko, E. V. SSZ-13 Zeolite with Isolated Co^{2+} Sites as an Efficient and Durable Catalyst System for Non-Oxidative Ethane Dehydrogenation. *Angew. Chem., Int. Ed.* **2026**, *65*, No. e19600.
(22) Shi, Q.; Song, Y.; Li, D.; Wang, Y.; Xie, Z.; Fan, X.; Kong, L.; Xiao, X.; Zhao, Z. Understanding the mechanism of propane dehydrogenation over coordinatively unsaturated Co-O acid-base pairs and the inhibition effect of trace oxygen. *J. Catal.* **2024**, *433*, No. 115472.
(23) Jeon, N.; Oh, J.; Tayal, A.; Jeong, B.; Seo, O.; Kim, S.; Chung, I.; Yun, Y. Effects of heat-treatment atmosphere and temperature on cobalt species in Co/Al_2O_3 catalyst for propane dehydrogenation. *J. Catal.* **2021**, *404*, 1007–1016.
(24) Hu, B.; Bean Getsoian, A.; Schweitzer, N. M.; Das, U.; Kim, H.; Niklas, J.; Poluektov, O.; Curtiss, L. A.; Stair, P. C.; Miller, J. T.; et al. Selective propane dehydrogenation with single-site CoII on SiO_2 by a non-redox mechanism. *J. Catal.* **2015**, *322*, 24–37.
(25) Hu, Z.-P.; Qin, G.; Han, J.; Zhang, W.; Wang, N.; Zheng, Y.; Jiang, Q.; Ji, T.; Yuan, Z.-Y.; Xiao, J.; et al. Atomic Insight into the Local Structure and Microenvironment of Isolated Co-Motifs in MFI Zeolite Frameworks for Propane Dehydrogenation. *J. Am. Chem. Soc.* **2022**, *144* (27), 12127–12137.
(26) Li, Y.; Zhang, Q.; Fu, S.; Kondratenko, V. A.; Otroshchenko, T.; Bartling, S.; Zhang, Y.; Zanina, A.; Wang, Y.; Cui, G. Active species and fundamentals of their creation in Co-containing catalysts for efficient propane dehydrogenation to propylene. *Chem. Eng. J.* **2023**, *460*, No. 141778.
(27) Wang, W.; Wu, Y.; Liu, T.; Zhao, Y.; Qu, Y.; Yang, R.; Xue, Z.; Wang, Z.; Zhou, F.; Long, J. Single Co sites in ordered SiO_2 channels for boosting nonoxidative propane dehydrogenation. *ACS Catal.* **2022**, *12* (4), 2632–2638.
(28) Jeon, N.; Seo, O.; Oh, J.; Park, J.; Chung, I.; Kim, J.; Sakata, O.; Tayal, A.; Yun, Y. Non-oxidative propane dehydrogenation over alumina-supported Co-V oxide catalysts. *Appl. Catal., A* **2021**, *614*, No. 118036.
(29) Li, J.; Zhang, Q.; He, G.; Zhang, T.; Li, L.; Li, J.; Hao, D.; Zhang, W.; Terasaki, O.; Mei, D.; et al. Silanol-Stabilized Atomically Dispersed $Pt^{\delta+}$-O_x-Sn Active Sites in Protozeolite for Propane Dehydrogenation. *J. Am. Chem. Soc.* **2024**, *146* (35), 24358–24367.
(30) Lee, S.; Kwon, H. C.; Jeong, J.; Shin, H.; Oh, D.; Seok, J.; Kim, J. C.; Choi, M. Ideal Bifunctional Catalysis for Propane Dehydrogenation over Pt-Promoted Gallia-Alumina and Minimized Use of Precious Elements. *J. Am. Chem. Soc.* **2025**, *147* (8), 6480–6491.
(31) Qin, D.; Cai, L.; Zhang, S.; Chu, W.; Yang, W. Zinc Doping Boosts the Reactivity and Anti-Coking Ability of Cobalt-Based Catalysts for Propane Dehydrogenation. *ACS Catal.* **2025**, *15*, 11794–11805.
(32) Zhang, X.; Liu, W.; Li, J.; Zhao, Y.; Tang, Z.; Xu, L.; Mu, R.; Li, X.; Zhu, X. Robust Subnano CoSn Ensembles for Selective Dehydrogenation of n-Butane. *ACS Catal.* **2025**, *15*, 13107–13117.
(33) Rennard, R. J.; Freel, J. The role of sulfur in deactivation of $PtMgAl_2O_4$ for propane dehydrogenation. *J. Catal.* **1986**, *98* (2), 235–244.
(34) Nakhaei Pour, A.; Shahri, S. M. K.; Bozorgzadeh, H. R.; Zamani, Y.; Tavasoli, A.; Marvast, M. A. Effect of Mg, La and Ca promoters on the structure and catalytic behavior of iron-based catalysts in Fischer−Tropsch synthesis. *Appl. Catal., A* **2008**, *348* (2), 201–208.
(35) Shi, J.; Zhou, Y.; Zhang, Y.; Zhou, S.; Zhang, Z.; Kong, J.; Guo, M. Synthesis of magnesium-modified mesoporous Al_2O_3 with enhanced catalytic performance for propane dehydrogenation. *J. Mater. Sci.* **2014**, *49* (16), 5772–5781.
(36) Wu, T.; Liu, G.; Zeng, L.; Sun, G.; Chen, S.; Mu, R.; Agbotse Gbonfoun, S.; Zhao, Z.-J.; Gong, J. Structure and catalytic consequence of Mg-modified VO_x/Al_2O_3 catalysts for propane dehydrogenation. *AIChE J.* **2017**, *63* (11), 4911–4919.
(37) Yang, L.; Yang, Y.; Song, S.; Fo, Y.; Ji, X.; Yang, K.; Liu, J.; Song, W. Alkaline-earth metals promote propane dehydrogenation with carbon dioxide through geometric effects: Altering the reaction pathway. *Appl. Catal., B* **2025**, *366*, No. 124985.
(38) Zhao, D.; Guo, K.; Han, S.; Doronkin, D. E.; Lund, H.; Li, J.; Grunwaldt, J.-D.; Zhao, Z.; Xu, C.; Jiang, G.; et al. Controlling Reaction-Induced Loss of Active Sites in ZnO_x/Silicalite-1 for Durable Nonoxidative Propane Dehydrogenation. *ACS Catal.* **2022**, *12* (8), 4608–4617.
(39) Zhao, D.; Li, Y.; Han, S.; Zhang, Y.; Jiang, G.; Wang, Y.; Guo, K.; Zhao, Z.; Xu, C.; Li, R.; et al. ZnO Nanoparticles Encapsulated in Nitrogen-Doped Carbon Material and Silicalite-1 Composites for Efficient Propane Dehydrogenation. *iScience* **2019**, *13*, 269–276.
(40) Ravel, B.; Newville, M. ATHENA, ARTEMIS, HEPHAESTUS: data analysis for X-ray absorption spectroscopy using *IFEFFIT*. *J. Synchrotron Radiat.* **2005**, *12* (4), 537–541.

https://doi.org/10.1021/acscatal.6c01078
ACS Catal. 2026, 16, 8543−8554

(41) Mallon, E. E.; Jeon, M. Y.; Navarro, M.; Bhan, A.; Tsapatsis, M. Probing the relationship between silicalite-1 defects and polyol adsorption properties. *Langmuir* **2013**, *29* (22), 6546–6555.
(42) Qi, L.; Babucci, M.; Zhang, Y.; Lund, A.; Liu, L.; Li, J.; Chen, Y.; Hoffman, A. S.; Bare, S. R.; Han, Y.; et al. Propane Dehydrogenation Catalyzed by Isolated Pt Atoms in ≡SiOZn−OH Nests in Dealuminated Zeolite Beta. *J. Am. Chem. Soc.* **2021**, *143* (50), 21364–21378.
(43) Wu, L.; Ren, Z.; He, Y.; Yang, M.; Yu, Y.; Liu, Y.; Tan, L.; Tang, Y. Atomically Dispersed Co^{2+} Sites Incorporated into a Silicalite-1 Zeolite Framework as a High-Performance and Coking-Resistant Catalyst for Propane Nonoxidative Dehydrogenation to Propylene. *ACS Appl. Mater. Interfaces* **2021**, *13* (41), 48934–48948.
(44) Liu, H.; Zhou, J.; Chen, T.; Hu, P.; Xiong, C.; Sun, Q.; Chen, S.; Lo, T. W. B.; Ji, H. Isolated Pt Species Anchored by Hierarchical-like Heteroatomic Fe-Silicalite-1 Catalyze Propane Dehydrogenation near the Thermodynamic Limit. *ACS Catal.* **2023**, *13* (5), 2928–2936.
(45) Han, D.; Liu, M.; Huang, C.; Sun, X.; Guan, L.; He, B.; Mei, Y.; Zu, Y. Uniformly stable hydroxylated cobalt(II) silicate species embedded within silicalite-1 zeolite for boosting propane dehydrogenation. *Microporous Mesoporous Mater.* **2023**, *352*, No. 112516.
(46) Song, S.; Zhao, M.; Barba-Nieto, I.; Fernández-García, M.; Chen, X.; Fo, Y.; Zhang, R.; Zhao, Z.; Concepción, P.; Liu, J.; et al. CO Adsorbates Induced Framework-Associated Low-Valence $Co^{\delta+}$ Sites in Co-ZSM-5 for Ethane Dehydrogenation. *J. Am. Chem. Soc.* **2025**, *147* (37), 33666–33678.
(47) Janas, J.; Shishido, T.; Che, M.; Dzwigaj, S. Role of tetrahedral Co(II) sites of CoSiBEA zeolite in the selective catalytic reduction of NO: XRD, UV−vis, XAS and catalysis study. *Appl. Catal., B* **2009**, *89* (1), 196–203.
(48) Estes, D. P.; Siddiqi, G.; Allouche, F.; Kovtunov, K. V.; Safonova, O. V.; Trigub, A. L.; Koptyug, I. V.; Copéret, C. C−H Activation on Co,O Sites: Isolated Surface Sites versus Molecular Analogs. *J. Am. Chem. Soc.* **2016**, *138* (45), 14987–14997.
(49) Corma, A. Inorganic Solid Acids and Their Use in Acid-Catalyzed Hydrocarbon Reactions. *Chem. Rev.* **1995**, *95* (3), 559–614.
(50) Tian, P.; Wei, Y.; Ye, M.; Liu, Z. Methanol to Olefins (MTO): From Fundamentals to Commercialization. *ACS Catal.* **2015**, *5* (3), 1922–1938.
(51) Ghazimoradi, M.; Soltanali, S.; Karami, H.; Ghassabzadeh, H.; Bakhtiari, J. A facile strategy to prepare ZSM-5-based composites with enhanced light olefin selectivity and stability in the HTO process. *RSC Adv.* **2023**, *13* (29), 20058–20067.
(52) Xu, W. Q.; Suib, S. L.; Oyoung, C. L. Studies of Acidic Sites on Boralites by Temperature-Programmed Desorption (TPD) of NH_3, C_2H_4, and 1-C_4H_8. *J. Catal.* **1993**, *144* (1), 285–295.
(53) Bagnasco, G. Improving the Selectivity of NH_3TPD Measurements. *J. Catal.* **1996**, *159* (1), 249–252.
(54) Cecilia, J. A.; Infantes-Molina, A.; Rodríguez-Castellón, E.; Jiménez-López, A.; Oyama, S. T. Oxygen-removal of dibenzofuran as a model compound in biomass derived bio-oil on nickel phosphide catalysts: Role of phosphorus. *Appl. Catal., B* **2013**, *136-137*, 140–149.
(55) Morales, R.; Campos, C. H.; Fierro, J. L. G.; Fraga, M. A.; Pecchi, G. Perovskite as nickel catalyst precursor − impact on catalyst stability on xylose aqueous-phase hydrogenation. *RSC Adv.* **2016**, *6* (72), 67817–67826.

https://doi.org/10.1021/acscatal.6c01078
ACS Catal. 2026, 16, 8543−8554